MOLECULAR IMAGING AND BIOLOGY

Mol Imaging Biol (2015) 17:565–574
DOI: 10.1007/s11307-015-0850-8

Published Online: 21 April 2015

RESEARCH ARTICLE

Initial Evaluation of [^{18}F]DCFPyL for Prostate-Specific Membrane Antigen (PSMA)-Targeted PET Imaging of Prostate Cancer

Zsolt Szabo,[1] Esther Mena,[1] Steven P. Rowe,[1] Donika Plyku,[1] Rosa Nidal,[2] Mario A. Eisenberger,[2] Emmanuel S. Antonarakis,[2] Hong Fan,[1] Robert F. Dannals,[1] Ying Chen,[1] Ronnie C. Mease,[1,2] Melin Vranesic,[1] Akrita Bhatnagar,[1] George Sgouros,[1,2] Steve Y. Cho,[1,3] Martin G. Pomper[1,2]

[1]*The Russell H. Morgan Department of Radiology and Radiological Science, Johns Hopkins Medical Institutions, Cancer Research Bldg. 2, Room 492, 1550 Orleans St, Baltimore, MD, 21231, USA*
[2]*Sidney Kimmel Comprehensive Cancer Center, Johns Hopkins Medical Institutions, Baltimore, MD, USA*
[3]*Department of Radiology, University of Wisconsin School of Medicine and Public Health, Madison, WI, USA*

Abstract

Purpose: Prostate-specific membrane antigen (PSMA) is a recognized target for imaging prostate cancer. Here we present initial safety, biodistribution, and radiation dosimetry results with [^{18}F]DCFPyL, a second-generation fluorine-18-labeled small-molecule PSMA inhibitor, in patients with prostate cancer.

Procedures: Biodistribution was evaluated using sequential positron-emission tomography (PET) scans in nine patients with prostate cancer. Time-activity curves from the most avid tumor foci were determined. The radiation dose to selected organs was estimated using OLINDA/EXM.

Results: No major radiotracer-specific adverse events were observed. Physiologic accumulation was observed in known sites of PSMA expression. Accumulation in putative sites of prostate cancer was observed (SUV_{max} up to >100, and tumor-to-blood ratios up to >50). The effective radiation dose from [^{18}F]DCFPyL was 0.0139 mGy/MBq or 5 mGy (0.5 rem) from an injected dose of 370 MBq (10 mCi).

Conclusions: [^{18}F]DCFPyL is safe with biodistribution as expected, and its accumulation is high in presumed primary and metastatic foci. The radiation dose from [^{18}F]DCFPyL is similar to that from other PET radiotracers.

Key words: PSMA, PET, Prostate cancer, Molecular imaging, Fluorine-18

Introduction

Prostate cancer is the most common cancer among men in the USA with an estimated number of new cases of 233,000 annually; it also represents the second most common cause of cancer-related death in men [1]. While often curable, there remain a large number of patients with residual, recurrent, and metastatic disease who need imaging for lesion detection, therapeutic monitoring, and restaging. Conventional anatomic and functional imaging including contrast-enhanced computed tomography (CT), [^{99m}Tc] methylene diphosphonate (MDP) bone scan, ultrasound, or

Correspondence to: Martin Pomper; *e-mail:* mpomper@jhmi.edu

magnetic resonance imaging (MRI) may not be sufficiently sensitive and specific for detection of prostate cancer lesions [2–5]. Positron emission tomography (PET) employing 2-deoxy-2-[18F]fluoro-D-glucose (FDG PET), the clinical standard for a number of other cancers, has demonstrated mixed results in imaging prostate cancer [6–9].

A number of new PET radiotracers have been introduced for imaging prostate cancer [10–15]. Proving particularly effective are low-molecular-weight agents that bind to the prostate-specific membrane antigen (PSMA), which is highly expressed in castration-resistant, metastatic prostate cancer [16–18]. We recently published the synthesis and first human imaging results of a selective low-molecular-weight inhibitor of PSMA, *N*-[*N*-[(*S*)-1,3-dicarboxypropyl]carbamoyl]-4-[18F]fluorobenzyl-L-cysteine ([18F]DCFBC) [19, 20]. Subsequently, similar urea derivatives radiolabeled with gallium-68 have been introduced by us [21] and others [22, 23].

Images obtained with [18F]DCFBC enabled reliable detection of lesions due to prostate cancer, yet they demonstrated considerable blood pool activity [20]. Such persistent blood pool activity could potentially interfere with the detection of lymph node metastases in the retroperitoneum and pelvis that are adjacent to large blood vessels. In part to address this potential limitation, we developed a second-generation low-molecular-weight, PSMA-targeted PET radiotracer, 2-(3-(1-carboxy-5-[(6-[18F]fluoro-pyridine-3-carbonyl)-amino]-pentyl)-ureido)-pentanedioic acid ([18F]DCFPyL, Fig. 1) [24]. Tissue binding of [18F]DCFPyL for PSMA (K_i=1.1±0.1 nM) is more than five times greater than the already high affinity of our first-generation radiotracer, [18F]DCFBC. Pre-clinical imaging with [18F]DCFPyL demonstrated PSMA(+) PC3 PIP to (isogenic) PSMA(−) PC3 flu tumor ratios exceeding 300:1 at 2 h post-injection with minimal non-target tissue uptake [24].

The goal of this first-in-human study was to investigate the safety, biodistribution, radiation dosimetry (including calculation of dose-limiting organ), and feasibility of tumor detection of [18F]DCFPyL in patients with known prostate cancer. Additionally, given the dynamic nature of the PET acquisitions performed, we hoped to gain insight into the optimum time point for imaging with this radiotracer.

Materials and Methods

Chemistry

DCFPyL was prepared according to a modification of a literature procedure [24] using 2,3,5,6-tetrafluorophenyl-6-fluoronicotinate [25] and (*S*)-di-*tert*-butyl 2-(3-((*S*)-6-amino-1-(*tert*-butoxy)-1-oxohexan-2-yL)ureido)pentanedioate formate salt [26] to provide a route that would conform to current good manufacturing practice (cGMP). *N*,*N*,*N*,-trimethyl-5-((2,3,5,6-tetrafluorophenoxy)carbonyl)pyridin-2-aminium trifluoromethanesulfonate was also prepared according to a modification of a literature procedure [27] to conform to cGMP.

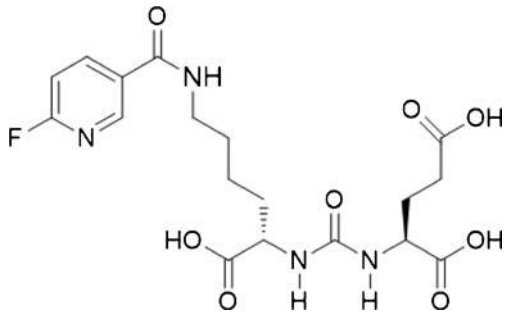

Fig. 1. Chemical structure of [18F]DCFPyL.

Radiochemistry

[18F]DCFPyL was prepared using a modified dual-run FDG synthesis module according to a modification of a previously published synthetic route [24]. Briefly, the F-18-labeled prosthetic group, 2,3,5,6-tetrafluorophenyl-6-[18F]fluoronicotinate (18F-FPy-TEP) was synthesized and purified by solid-phase extraction, followed by coupling to (*S*)-di-*tert*-butyl 2-(3-((*S*)-6-amino-1-(*tert*-butoxy)-1-oxohexan-2-yL)ureido)pentanedioate formate salt and acid hydrolysis to afford [18F]DCFPyL with an average non-decay-corrected radiochemical yield from [18F]fluoride of 2.8 ±1.2 %, specific activity of 159±45 GBq/μmol (4298±1228 Ci/mmol), and 100 % radiochemical purity (n=9). The average time of synthesis was 90 min. [18F]DCFPyL was eluted from the purification cartridge with 1 ml of ethanol followed by 10 ml of 0.9 % sodium chloride *via* a sterilizing 0.22 μm filter into a sterile vial containing 4 ml of 0.9 % sodium chloride. We required ≥95 % chemical purity for human administration of [18F]DCFPyL.

Patients

This study was approved by the Institutional Review Board at our institution. Written consent was obtained from each patient. Human research was also approved by the FDA under the auspices of an exploratory investigational new drug application (eIND # 121,064). Patients were recruited from the Johns Hopkins Prostate Cancer/Genitourinary Oncology Program. Key inclusion criteria were as follows: greater or equal to 18 years of age, histologic confirmation of prostate cancer, radiologic evidence of new or progressive metastatic disease demonstrated on anatomic imaging (CT, MRI, or ultrasound), bone scintigraphy, sodium [18F]fluoride PET, or [18F]FDG PET, and prostate-specific antigen (PSA) blood levels of 1 ng/ml or higher. Patients could be on androgen deprivation therapy if dose was stable for ≥1 week. Other inclusion criteria included the following: platelet count>50,000/mm^3; neutrophil count>1000/mm^3; the patient was judged by the investigator to have the initiative and means to be compliant with the protocol; the patient or their legal representative must have had the ability to read, understand, and provide written informed consent for the initiation of any study-related procedures. Out of the total of nine patients, eight patients met these inclusion criteria.

One of the patients lacked evidence of disease on conventional imaging and was found to have a PSA value of only 0.1 ng/ml (though this value may have been relatively depressed by treatment with androgen deprivation). There was strong clinical suspicion for

recurrent disease in the pelvis in this patient on the basis of a palpable abnormality on digital rectal exam.

Exclusion criteria included the following: (1) Karnofsky performance status of <60; (2) inadequate venous access; (3) permanent prostate brachytherapy implant; (4) another radioisotope administered within five physical half-lives prior to study enrollment; (5) serum creatinine >3 times the upper limit of normal; (6) total bilirubin >3 times the upper limit of normal; (7) liver transaminases >5 times the upper limit of normal; (8) treatment with an investigational drug, investigational biologic, or investigational therapeutic device within 30 days prior to study; (9) radiation therapy or chemotherapy within 2 weeks prior to study; and (10) prior history of any other malignancy within 3 years, other than basal cell carcinoma of the skin. Pre-study and post-study evaluations performed within 2 weeks of administration of [18F]DCFPyL included as follows: medical history and physical examination with vital signs, laboratory tests (complete blood count (CBC) with differential and a comprehensive metabolic panel to include blood urea nitrogen (BUN), creatinine, alkaline phosphatase, total bilirubin, and liver transaminase levels), and ECG.

Study Procedures

Patients were identified and proposed by their treating physicians. Eligibility was verified, and a study investigator reviewed the study with the patient and obtained written consent. Patients fasted for 4–6 h prior to injection of [18F]DCFPyL, which is our standard protocol prior to imaging with FDG although the necessity of fasting or non-fasting status has not been established with [18F]DCFPyL. Vital signs (blood pressure, heart rate, respiratory rate) and ECG were taken prior to administration of the radiotracer, and continuous monitoring with pulse oximetry was performed during PET/CT scanning.

Two intravenous (IV) peripheral catheters were placed, one for radiotracer injection and one on the contralateral arm for withdrawal of blood samples. Patients were asked to void prior to administration of [18F]DCFPyL, between the fourth and fifth PET scans, and after the fifth PET scan. Urine samples were collected for measurement of excreted radioactivity.

An average bolus of 320.6 MBq (8.66 mCi, range 310.8–327.1 MBq (8.40–8.84 mCi)) of [18F]DCFPyL was injected by slow IV push. The average administered specific activity was 107.2 MBq/nmol (2.90 Ci/μmol, range 85.8–141.0 MBq/nmol (2.32–3.81 Ci/μmol)).

PET/CT scans were performed on a Discovery DRX PET/CT scanner (GE Healthcare, Waukesha, WI, USA) operating in three-dimensional (3D) emission acquisition mode and using CT for attenuation correction. A low-dose CT scan was performed followed by four sequential PET scans from the mid thigh to the skull vertex (including 7 to 8 fields-of-view depending on patient height) beginning immediately post-radiotracer injection. For the first of these PET scans, imaging was performed for 1 min per bed position, while for the second PET scan, imaging was performed for 2 min per bed position, and for the third and fourth scans, imaging was performed for 4 min per bed position. These acquisitions are labeled as PET1 through PET4 for the duration of this manuscript. After PET4, the patient was asked to void and a urine sample was collected. At 120 min following the injection of [18F]DCFPyL (usually, approximately 30 min after PET4), a second low-dose CT was obtained followed by a fifth 3D PET acquisition (PET5) at 4 min per bed position.

Blood samples were obtained from the vein contralateral to the site of injection for evaluation of biodistribution and metabolism at three time points: (1) after PET2, (2) after PET4, and (3) after the completion of PET5.

Nine patients returned within 30 days after [18F]DCFPyL PET/CT imaging for a follow-up history, physical examination, routine blood chemistry analysis, and ECG. A study member contacted one patient within 30 days after the [18F]DCFPyL PET/CT imaging study to query about late-occurring adverse events.

Image Analysis

The PET/CT images were visually reviewed on a MIM workstation (MIM Software, Cleveland, Ohio) by two readers board certified in nuclear medicine (ZS and SYC). The readers were not blinded to the identities or clinical histories of the patients. PET5 time point PET/CT foci of increased radiotracer uptake compared to surrounding soft tissue or blood pool were determined to be sites of suspected tumor, either with or without corresponding detectable tumor by correlative conventional imaging. Tumor uptake expressed as maximum standardized uptake value normalized to lean body mass (SUV_{max}) was used in each lesion to characterize tumor radiotracer uptake for the hottest tumor lesions in each patient (maximum of five lesions per patient). For this purpose, volumes of interest (VOIs) were drawn automatically at 50 % activity threshold of each lesion. Tumor-to-reference tissue was calculated as the ratio of lesion SUV_{max} divided by SUV_{mean} of the liver, blood pool, and muscle.

Radiation Dosimetry

Detailed dosimetry calculations were performed on four patients as described. The Medical Internal Radiation Dose (MIRD) *S* value schema [28] as implemented in the software code OLINDA/EXM (Vanderbilt University) [29] was used to perform the absorbed dose calculations as described previously [20]. Time-integrated activity coefficients (TIACs) (*i.e.*, residence times) were obtained by drawing volumes of interest (VOIs) corresponding to each of the organs that could be positively identified on longitudinal PET scans. In most cases, the VOI covered the entire organ volume. For cases in which the entire organ volume could not be separated from adjacent structures, a smaller VOI was drawn to estimate the organ concentration. Total organ activity or activity concentration was integrated either by analytically integrating a fitted single or double-exponential function to the measured data or by numerical integration and then extrapolation based on a single exponential fit to the last four or five data points. Whole organ TIACs were divided by patient-specific organ masses obtained using CT VOIs and reference organ densities [30]. These were then multiplied by the reference organ masses listed in the OLINDA/EXM software to give scaled organ TIACs appropriate to the reference geometry used in OLINDA/EXM; TIACs concentrations were directly multiplied by the OLINDA/EXM organ masses. The MIRD bladder model [31] was used to calculate the absorbed dose to the bladder with a voiding interval of 1.5 h, the biological whole-body clearance half-life, and a fraction of 1. The absorbed dose to the lens of the eye was estimated as equivalent to the photon absorbed

dose to the brain. The absorbed dose to tissues that showed activity accumulation such as the lacrimal, parotid, and submandibular glands was calculated as the sum of the electron (positron) dose contribution and the total photon dose contribution from the brain to lens and glands and remainder body to brain. Monte-Carlo models using Geant4 are being developed to confirm the accuracy of these estimates and will be reported separately.

Blood and Plasma Activity, Plasma Metabolites

Blood and plasma activities were measured in a well-type counter using 0.5 ml aliquots collected from five subjects at the following time points: post-PET 2, post-PET 4, and post-PET 5. Each patient was asked to empty his bladder after PET4 and after PET5. Thus, urinary excretion was calculated at approximately 110 min and at approximately 160 min post-injection. Radiotracer metabolites in plasma were determined in three patients. For this purpose, plasma proteins were precipitated from plasma samples from the blood obtained post-PET 2, post-PET 4, and post-PET 5 (approximately 34, 110, and 160 min post-injection, respectively) by the addition of acetonitrile followed by centrifugation. The supernatant was spiked with non-radiolabeled DCFPyL, diluted with triethylammonium phosphate buffer (pH 3.2), and injected onto the radio-HPLC for analysis using a Gemini 4.6×250 mm C18 column (Phenomenex, Torrance, CA), and a mobile phase of 10 % acetonitrile/90 % triethylammonium phosphate (pH 3.2) at an elution rate of 2 ml/min.

Results

Patients

Patients were an average of 70 years of age (range 63–79 years), with an average weight of 82 kg (range 79–84 kg) and an average height of 175 cm (range 168–183 cm). The Gleason score at first diagnosis was 7 in four subjects, 9 in four subjects, and 10 in one subject. The PSA value within a ±1 week time window from the date of PET imaging was 8.00 ng/ml (range 5.30–30.48 ng/ml). Individual PSA values and Gleason scores together with pertinent clinical information are listed in Table 1.

Adverse Events

Patients have not experienced any severe adverse events. One patient reported two adverse events that were classified as unlikely to be attributable to the radiotracer (mild headache and mild nose bleed, both of which resolved without treatment and were considered grade I by the National Cancer Institute Common Terminology Criteria for Adverse Events (NCI CTCAE) Version 4.0). Another participant experienced a decrease in platelet count on routine assessment during the post-imaging follow-up which, at the time of publication, had not resolved but which was attributed to the participant starting treatment for prostate cancer. This was also a NCI CTCAE grade I adverse event. There were no radiotracer-related adverse events with monitored heart rate or blood pressure.

Biodistribution

Maximum intensity projection (MIP) images (representative patient shown in Fig. 2) demonstrated physiologic radiotracer accumulation in the salivary glands, lacrimal glands, liver, spleen, and (predominantly small) intestines. Average time-activity curves for the organs that were dosimetrically evaluated are shown in Fig. 3. There was rapid washout of activity from the blood pool and significant renal excretion with radiotracer accumulation in the bladder. No radiotracer uptake was seen in the brain. The pattern of physiologic biodistribution was not visually affected by the presence of metastatic disease (Fig. 4 shows serial MIPs of a patient with numerous sites of suspected bone and lymph node prostate cancer metastases; in comparison to Fig. 2, in which the patient only had a single site of abnormal uptake in the pelvis that is not well demonstrated on the MIPs, there is no appreciable difference in the visible biodistribution).

Table 1. Selected demographic and clinical information for the patients included in this study

Patient	Age	PSA (ng/ml)	Gleason	Medical history
1	67	8.6	9	Prior radical prostatectomy, radiotherapy, and androgen deprivation.
2	63	11	7	Prior external beam radiation therapy with evidence of biochemical relapse on testosterone suppression therapy.
3	51	0.1	9	Prior radical prostatectomy. Ongoing androgen deprivation therapy. Marginal PSA response.
4	85	26.2	7	Prior external-beam radiotherapy.
5	62	6	7	Prior radical prostatectomy and salvage external beam radiation therapy. Biochemical relapse.
6	77	5.3	10	Prior radical prostatectomy and radiation therapy and multiple research treatment protocols in the past.
7	73	204.8	9	Prior radical prostatectomy with prior treatment with androgen deprivation therapy and multiple chemotherapy trials, though PSA has continued to increase.
8	88	5.08	7	Metastatic hormone-sensitive prostate cancer status post approximately 18 months of androgen deprivation, who is now off treatment with a slowly rising PSA.
9	73	8	9	Metastatic prostate cancer status post radiation therapy to the left hemipelvis in addition to hormonal therapy. Rising PSA.

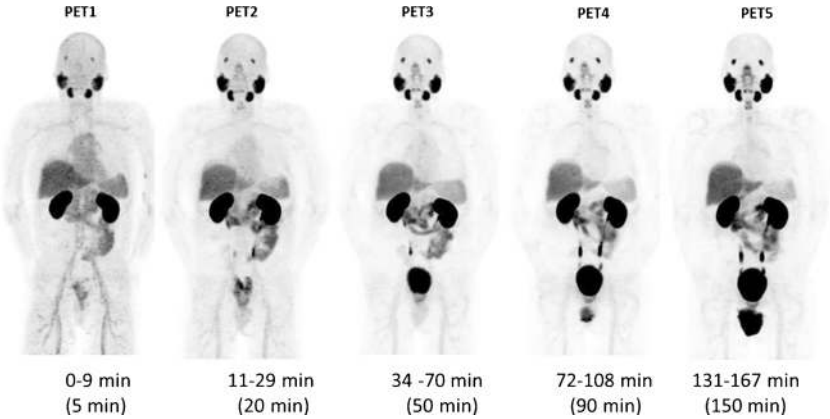

Fig. 2. Maximum intensity projection (*MIP*) PET image sequence in patient # 3. This patient demonstrated physiologic tracer uptake in the salivary glands, lacrimal glands, kidneys, liver, spleen, small intestine, and urinary excretion. There was uptake also in a histologically confirmed metastatic lesion involving the rectal wall.

Blood and Plasma Activity, Plasma Metabolites

Red cell binding of the radiopharmaceutical was negligible at 20 min and non-detectable at 86 and 137 min post-injection (Fig. 5).

Analysis of plasma samples by high-performance liquid chromatography (HPLC) up to 173 min post-injection demonstrated that all plasma activities were in the form of unmetabolized radioligand (Fig. 6). Average urinary excretion of the radiotracer was 11 % (range 6–15 %) by 2 h and 16 % (range 8–21 %) by 3 h post-injection. In the three patients studied, no metabolism of [18F]DCFPyL was observed on radio-HPLC analysis. All of the radioactivity co-eluted at the same retention time as non-radiolabeled DCFPyL.

Radiation Dosimetry

Detailed organ dosimetry derived from four representative patients is included in Table 2. Of note, the effective dose from [18F]DCFPyL was 0.0165 mSv/MBq or 6.1 mGy (0.61 rem) for an injected dose of 370 MBq (10 mCi). Highest radiation dose was estimated for the kidneys (0.0945 mGy/MBq) followed by urinary bladder wall (0.0864 mGy/MBq), submandibular glands (0.0387 mGy/MBq), and liver (0.0380 mGy/MBq). The mean absorbed dose to the bone marrow was 0.01 mGy/MBq. Residence times for selected organs are included in Table 3.

In comparison to the published data on [18F]DCFBC [20], [18F]DCFPyL shows significantly lower doses in most radiosensitive organs such as the thymus, osteogenic cells, red marrow, breast, testes, uterus and ovaries (though hypothetical in the context of an all-male patient cohort, we include calculated breast, uterus and ovarian dose so that the presented results may be more easily extrapolated to non-prostate cancer applications of this radiotracer). Less radiation dose was also measured in the stomach wall, small intestine, large intestinal wall, lungs, heart wall, brain, skin, muscle, thyroid and gallbladder wall. Radiation dose from [18F]DCFPyL was higher in the kidneys, adrenals, urinary bladder wall, liver, pancreas and spleen.

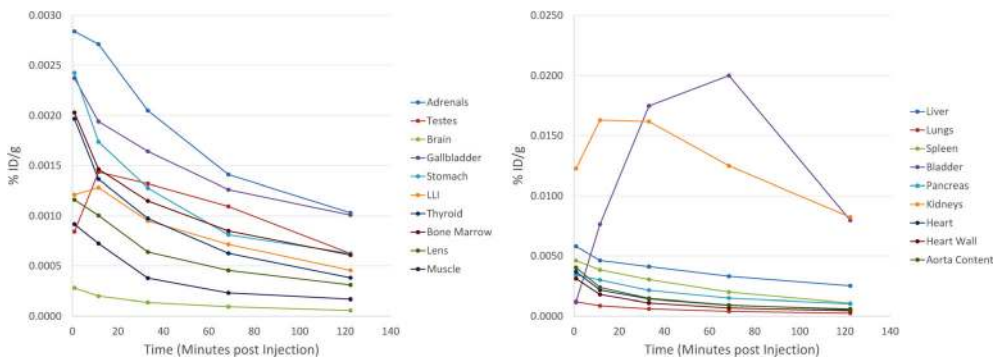

Fig. 3. Time-activity curves in selected organs expressed as percent of injected dose per gram tissue (%ID/g) as a function of time (in minutes) post-injection. Organs of low and high radiotracer uptake are shown in the left set and right set of time-activity curves, respectively.

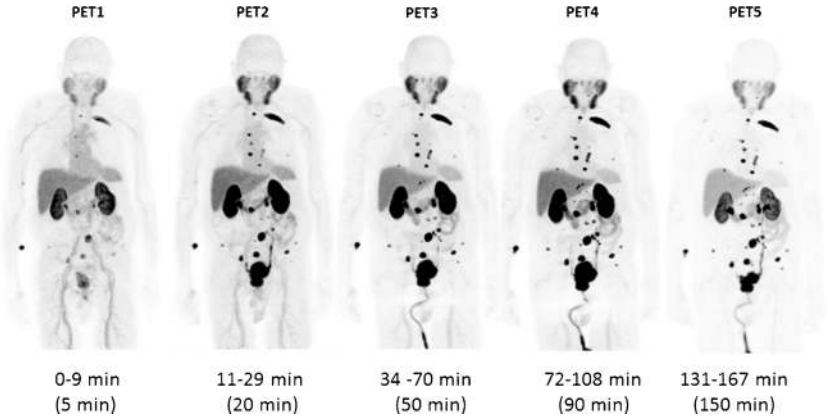

Fig. 4. Maximum intensity (*MIP*) PET image sequence in subject # 4. This patient demonstrated radiotracer binding in a large number of metastatic lesions involving multiple bones and lymph nodes. Physiologic biodistribution was the same as in the patient with minimal disease shown in Fig. 2.

Tumor Uptake

Visually, very high levels of uptake were observed in sites of putative metastatic disease, as well as in primary tumors in patients that had not undergone prostatectomy. In conjunction with the very low blood pool activity of [^{18}F]DCFPyL, the conspicuity of lesions was notably higher than with our first-generation radiotracer, [^{18}F]DCFBC. The overall uptake within the putative tumors increased from PET1 through PET5 (see Fig. 7 for representative tumor time-activity curves). The most [^{18}F]DCFPyL-avid bone lesions demonstrated SUV_{max} as high as 102.0 at the PET5 time point. Further, the most avid [^{18}F]DCFPyL-positive lymph node lesion had an SUV_{max} of 100.3 on PET5. The highest uptake we observed at a site of primary disease had an SUV_{max} of 71.6 on PET5. The tumor-to-blood and the tumor-to-muscle ratios increased from PET1 to PET5 while the tumor-to-liver ratio increased from PET1 to PET4 but declined in PET5 (Fig. 7). It is notable that high tumor uptake was achieved visually on both PET4 and PET5, with individual lesions demonstrating SUV_{max} greater than 100 at both approximately 1 and 2 h post-radiotracer injection, respectively.

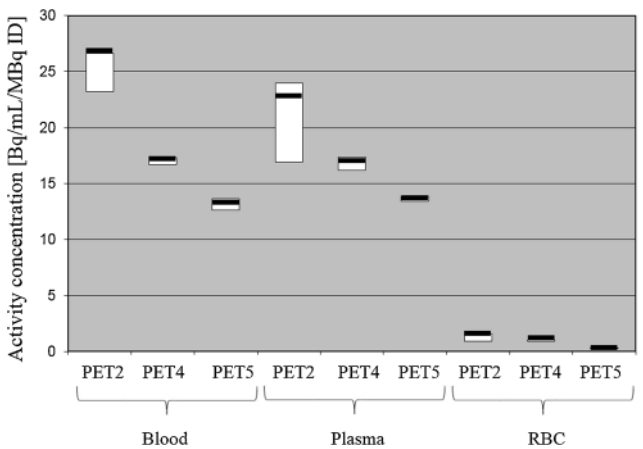

Fig. 5. Average blood activity, plasma activity, and red cell activity of [^{18}F]DCFPyL measured in nine subjects at 25, 86, and 150 min post-radiotracer administration.

No metastatic foci were observed in the liver or lungs. Patient # 3, with the lowest PSA value of 0.1 ng/μl, had only one detectable lesion in the rectal wall that was confirmed by biopsy. Patient # 7 had the highest PSA value of 204.8 ng/μl and had numerous positive lesions. A more comprehensive report of sites of suspected metastases visualized with [^{18}F]DCFPyL as well as comparison to conventional imaging will be reported separately.

Discussion

This first-in-man evaluation of the second-generation F-18-labeled, PSMA-targeted radiotracer [^{18}F]DCFPyL demonstrated a number of important findings. First, this radiotracer is safe to administer with only three NCI CTCAE grade I adverse events observed in the nine patients in this study, all of which were thought to be unlikely to be attributed to radiotracer administration.

Further, the biodistribution of [^{18}F]DCFPyL in humans parallels the expected uptake based upon the known distribution of PSMA. For example, uptake was high in the salivary glands, likely reflecting the high density of PSMA in these organs. Uptake was also high in the kidneys, which may be in part caused by specific PSMA binding [32] and in part by urinary excretion of the radiotracer, which resulted in accumulation within the urinary bladder. High activity in the salivary glands, kidneys, and bladder has been also observed with Ga-68-labeled PSMA-targeted radioligands [33–35].

Accumulation of [^{18}F]DCFPyL in putative foci of prostate cancer was rapid and very high with some lesions demonstrating SUV_{max} greater than 100. These exceptionally high SUV_{max} numbers are comparable to the uptake reported in some metastatic prostate cancer sites evaluated with Ga-68-labeled PSMA-targeted ligands. This uptake also compares favorably to our previously reported first-generation radiofluorinated ligand. In particular, the maximum tumor uptake to average blood pool uptake ratios seen

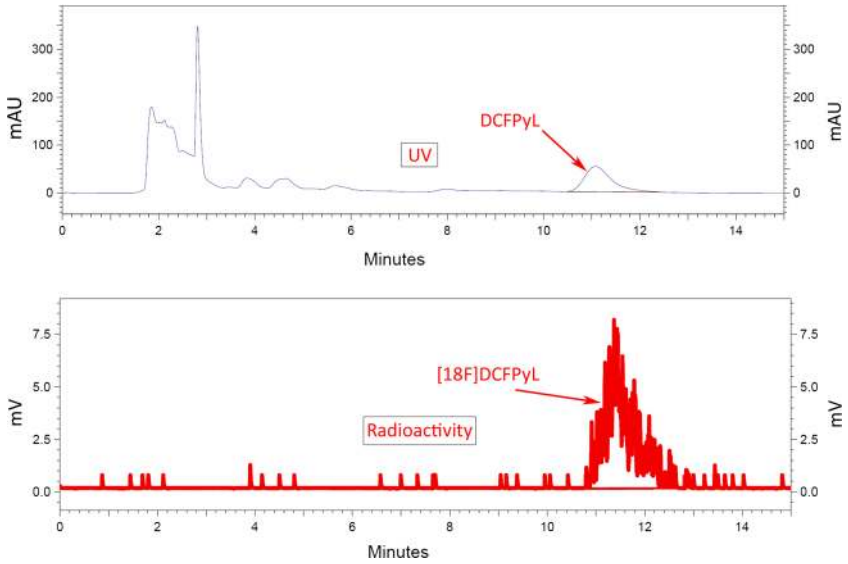

Fig. 6. HPLC curves of the plasma radiotracer ("*radioactivity*") in a subject at 34 and 173 min post-injection in comparison with the reference standard ligand ("*UV*").

with [18F]DCFPyL (an average of at least 10:1 for all representative lesion types, Fig. 7) are notably higher than the same ratios observed with our first-generation radiotracer (average <4:1 for all representative lesion types [20]). Rapid plasma clearance and low accumulation in the liver and muscle as compared to tumors result in very high tumor-to-background ratios. High target accumulation was likely due to the internalization of the radiotracer-PSMA complex [36].

Table 2. Radiation dose estimates for [18F]DCFPyL

Organ	Absorbed dose (mGy/MBq)
Adrenals	3.11E-02
Brain	2.19E-03
Breasts	4.57E-03
Gallbladder wall	1.44E-02
Heart wall	1.29E-02
Kidneys	9.45E-02
Lacrimal glands	3.50E-02
Lens	1.25E-03
Liver	3.80E-02
LLI wall	1.05E-02
Lungs	1.08E-02
Muscle	6.32E-03
Osteogenic cells	9.58E-03
Ovaries	8.89E-03
Pancreas	2.44E-02
Parotid glands	2.68E-02
Red marrow	1.04E-02
Skin	4.05E-03
Small intestine	9.13E-03
Spleen	1.85E-02
Stomach wall	1.16E-02
Submandibular glands	3.87E-02
Testes	1.01E-02
Thymus	5.56E-03
Thyroid	8.56E-03
ULI wall	1.67E-02
Urinary bladder wall	8.64E-02
Uterus	1.15E-02

Overall, these factors contributed to significantly improved visual conspicuity of suspected sites of metastatic prostate cancer in comparison to our first-generation radiotracer; for example, the low blood pool activity allowed for the definitive identification of presumed metastatic lymph nodes that were adjacent to large blood vessels in the retroperitoneum and pelvis. Other favorable features included very low red blood cell binding and the lack of radioactive metabolites circulating in plasma.

Visually, both PET4 and PET5 demonstrated high tumor uptake with relatively low blood pool, although a small number of small lesions became visible only on PET5. This suggests that imaging at approximately 1 h post-injection (similar to most clinical protocols with [18F]FDG) would be likely to evaluate the full extent of disease in most patients. However, in certain clinical situations, such as those patients presenting with new biochemical recurrence who may have a low disease burden, if no convincing evidence of a disease site is noted at the 1 h time point, delayed imaging at 2 h may be valuable. Particularly at later imaging time points, radiotracer activity in the urinary bladder became substantial (Fig. 4), which could conceivably obscure lesions adjacent to the bladder. In practice, we encourage patients to remain orally well hydrated and we also administer intravenous fluids to dilute accumulating activity in the bladder as much as possible. It has also become a part of our clinical protocol to begin whole-body PET acquisitions in patients being imaged with [18F]DCFPyL starting with the mid thighs as the first bed position and proceeding cranially; this ensures that bladder activity is as low as possible at the time the pelvis is being acquired.

The radiation dose in the whole body and radiosensitive organs such as the red marrow, gonads, and breasts was low (0.01 mGy/MBq or less). Only men were included in this

Table 3. Residence times for [18F]DCFPyL in selected organs

Organ	Res. time (Bq-h)/Bq
Adrenals	3.16E-04
Bone marrow (spine)	5.52E-02
Brain	4.74E-03
Gallbladder	1.18E-03
Heart	1.98E-02
Heart wall	6.24E-03
Kidneys	2.17E-01
Lacrimal glands	3.86E-04
Lens	4.32E-06
Liver	2.60E-01
LLI	4.06E-03
Lungs	3.70E-02
Muscle	3.07E-01
Pancreas	3.05E-03
Parotid glands	1.19E-02
Spleen	2.07E-02
Stomach	1.07E-02
Submandibular glands	6.95E-03
Testes	1.76E-03
Thyroid	2.34E-04
ULI	2.20E-02
Urinary bladder contents	2.60E-01
Total body	1.96E+00
Remainder of body	7.11E-01

study, so the listed radiation dose estimates for ovaries and breasts were based on the assumption that biodistribution in women is similar to biodistribution in men. The radiation dose was within limits required for research studies under an FDA Radioactive Drug Research Committee RDRC protocol [37] and was comparable to the radiation dose of other radiotracers used in oncology such as [18F]FDG [38].

[18F]DCFPyL demonstrated favorable dosimetry with significantly lower doses to most radiosensitive organs in comparison to our first-generation radiofluorinated ligand. At the time of the preparation of the present manuscript, no data were available on the radiation dose from Ga-68-labeled PSMA ligands. However, the effective radiation dose from another Ga-68-labeled radiotracer, [68Ga]DOTATATE, is two times higher [39]. Compared to the recently published PSMA radiotracer [124I]MIP [40], the radiation dose from [18F]DCFPyL was at least one order of magnitude lower in all measured organs, including whole body and radiosensitive organs.

A recent retrospective analysis of Ga-68 PSMA imaging studies of 319 patients resulted in lesion-based sensitivity, specificity, and negative predictive (NPV) and positive predictive (PPV) values of 76.6, 100, 91.4, and 100 % and

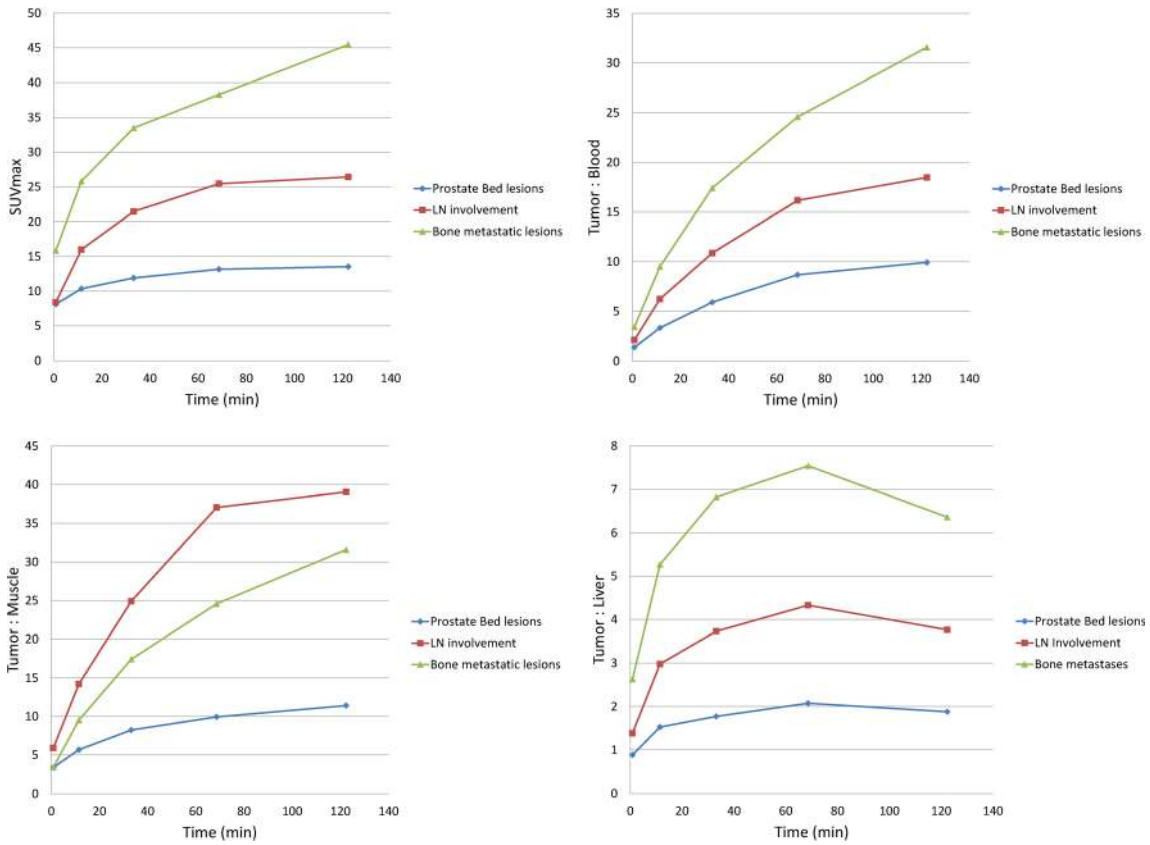

Fig. 7. Time course of tumor uptake values and tumor-to-background ratios. The time sequence of tumor uptake is expressed in SUV_{max} normalized to lean body mass (*left upper corner*). Tumor-to-blood ratios (*T*:*B*), tumor-to-muscle (*T*:*M*) ratios and tumor-to-liver (*T*:*L*) ratios are expressed in tumor SUV_{max}/reference tissue SUV_{mean}. The *graphs* show separately the average results from prostate bed lesions, lymph node metastases, and bone metastases (the hottest lesions from each patient were selected for this analysis, up to five lesions per patient).

a patient-based sensitivity of 88 % [41]. We have given preference to radiolabeling with F-18 since it may allow centralized production and commercial distribution and eliminate the need for on-site radiolabeling. Imaging with ^{18}F may also result in higher image resolution and lesion detectability [42]. Our findings with [^{18}F]DCFPyL, notably the comparable tumor uptake and low blood pool activity, suggest that this radiotracer would also be of comparable diagnostic utility to the Ga-68 agents, although ultimately, a direct comparison would be necessary to assess this supposition definitively.

Conclusion

Data from this initial clinical experience demonstrate that PET imaging with [^{18}F]DCFPyL is feasible and safe. Physiologic accumulation of the radiotracer corresponds to the distribution of PSMA-expressing organs and excretion. Accumulation in primary tumor and metastatic lesions is very high, which may permit the prospective detection of residual tumor as well as regional or distant metastases with high sensitivity and specificity. Radiation dose is within limits for diagnostic radiotracers for PET.

Acknowledgments. We are grateful for the efforts of Yavette Morton and Akimosa Jeffrey-Kwanisai in helping to coordinate this study. We acknowledge the financial support from the Prostate Cancer Foundation–Young Investigator Award, The Patrick C. Walsh Prostate Cancer Research Fund, EB006351, CA134675, CA184228, CA103175, CA183031, and CA116477.

Conflict of Interest. The authors declare that they have no conflicts of interest.

Funding. Prostate Cancer Foundation–Young Investigator Award, The Patrick C. Walsh Prostate Cancer Research Fund, EB006351, CA134675, CA184228, CA103175, CA183031.

Disclosures. None.

References

1. Siegel R, Ma J, Zou Z, Jemal A (2014) Cancer statistics. CA Cancer J Clin 64:9–29
2. Shinohara K, Wheeler TM, Scardino PT (1989) The appearance of prostate cancer on transrectal ultrasonography: correlation of imaging and pathological examinations. J Urol 142:76–82
3. Hricak H, Dooms GC, Jeffrey RB et al (1987) Prostatic carcinoma: staging by clinical assessment, CT, and MR imaging. Radiology 162:331–336
4. Scheidler J, Hricak H, Vigneron DB et al (1999) Prostate cancer: localization with three-dimensional proton MR spectroscopic imaging—clinicopathologic study. Radiology 213:473–480
5. Blomqvist L, Carlsson S, Gjertsson P et al (2014) Limited evidence for the use of imaging to detect prostate cancer: a systematic review. Eur J Radiol 83:1601–1606
6. Turlakow A, Yeung HW, Pui J et al (2001) Fludeoxyglucose positron emission tomography in the diagnosis of giant cell arteritis. Arch Intern Med 161:1003–1007
7. Hofer C, Laubenbacher C, Block T (1999) Fluorine-18-fluorodeoxyglucose positron emission tomography is useless for the detection of local recurrence after radical prostatectomy. Eur Urol 36:31–35
8. Nunez R, Macapinlac HA, Yeung HW et al (2002) Combined ^{18}F-FDG and 11C-methionine PET scans in patients with newly progressive metastatic prostate cancer. J Nucl Med 43:46–55
9. Shreve PD, Grossman HB, Gross MD, Wahl RL (1996) Metastatic prostate cancer: initial findings of PET with 2-deoxy-2-[F-18]fluoro-D-glucose. Radiology 199:751–756
10. Hricak H, Choyke PL, Eberhardt SC et al (2007) Imaging prostate cancer: a multidisciplinary perspective. Radiology 243:28–53
11. Lawrentschuk N, Davis ID, Bolton DM, Scott AM (2006) Positron emission tomography and molecular imaging of the prostate: an update. BJU Int 97:923–931
12. de Jong IJ, Pruim J, Elsinga PH et al (2003) ^{11}C-choline positron emission tomography for the evaluation after treatment of localized prostate cancer. Eur Urol 44:32–38, **Discussion 8–9**
13. Picchio M, Messa C, Landoni C et al (2003) Value of [^{11}C]choline-positron emission tomography for re-staging prostate cancer: a comparison with [^{18}F]fluorodeoxyglucose-positron emission tomography. J Urol 169:1337–1340
14. Scattoni V, Picchio M, Suardi N et al (2007) Detection of lymph-node metastases with integrated [11C]choline PET/CT in patients with PSA failure after radical retropubic prostatectomy: results confirmed by open pelvic-retroperitoneal lymphadenectomy. Eur Urol 52:423–429
15. Greco C, Cascini GL, Tamburrini O (2008) Is there a role for positron emission tomography imaging in the early evaluation of prostate cancer relapse? Prostate Cancer Prostatic Dis 11:121–128
16. Chang SS (2004) Overview of prostate-specific membrane antigen. Rev Urol 6(Suppl 10):S13–S18
17. Wright GL Jr, Grob BM, Haley C et al (1996) Upregulation of prostate-specific membrane antigen after androgen-deprivation therapy. Urology 48:326–334
18. Silver DA, Pellicer I, Fair WR et al (1997) Prostate-specific membrane antigen expression in normal and malignant human tissues. Clin Cancer Res 3:81–85
19. Mease RC, Dusich CL, Foss CA et al (2008) N-[N-[(S)-1,3-Dicarboxypropyl]carbamoyl]-4-[^{18}F]fluorobenzyl-L-cysteine, [^{18}F]DCFBC: a new imaging probe for prostate cancer. Clin Cancer Res 14:3036–3043
20. Cho SY, Gage KL, Mease RC et al (2012) Biodistribution, tumor detection, and radiation dosimetry of ^{18}F-DCFBC, a low-molecular-weight inhibitor of prostate-specific membrane antigen, in patients with metastatic prostate cancer. J Nucl Med 53:1883–1891
21. Banerjee SR, Pullambhatla M, Byun Y et al (2010) ^{68}Ga-labeled inhibitors of prostate-specific membrane antigen (PSMA) for imaging prostate cancer. J Med Chem 53:5333–5341
22. Eder M, Schafer M, Bauder-Wust U et al (2012) ^{68}Ga-complex lipophilicity and the targeting property of a urea-based PSMA inhibitor for PET imaging. Bioconjug Chem 23:688–697
23. Baur B, Solbach C, Andreolli E et al (2014) Synthesis, radiolabelling and in vitro characterization of the gallium-68-, yttrium-90- and lutetium-177-labelled PSMA ligand, CHX-A″-DTPA-DUPA-Pep. Pharmaceuticals 7:517–529
24. Chen Y, Pullambhatla M, Byun Y et al (2011) 2-(3-{1-Carboxy-5-[(6-[^{18}F]fluoro-pyridine-3-carbonyl)-amino]-pentyl}-urei do)-pentanedioic acid, [^{18}F]DCFPyL, a PSMA-based PET imaging agent for prostate cancer. Clin Cancer Res 17:7645
25. Olberg DE, Arukwe JM, Grace D et al (2010) One step radiosynthesis of 6-[(18)F]fluoronicotinic acid 2,3,5,6-tetrafluorophenyl ester ([(18)F]F-Py-TFP): a new prosthetic group for efficient labeling of biomolecules with fluorine-18. J Med Chem 53:1732–1740
26. Maresca KP, Hillier SM, Femia FJ et al (2009) A series of halogenated heterodimeric inhibitors of prostate specific membrane antigen (PSMA) as radiolabeled probes for targeting prostate cancer. J Med Chem 52:347–357
27. Bachner M, Loriot Y, Gross-Goupil M et al (2012) 2-(1)(8)fluoro-deoxy-D-glucose positron emission tomography (FDG-PET) for post-chemotherapy seminoma residual lesions: a retrospective validation of the SEMPET trial. Ann Oncol 23:59–64
28. Bolch WE, Eckerman KF, Sgouros G, Thomas SR (2009) MIRD pamphlet No. 21: a generalized schema for radiopharmaceutical dosimetry—standardization of nomenclature. J Nucl Med 50:477–484
29. Stabin MG, Sparks RB, Crowe E (2005) OLINDA/EXM: the second-generation personal computer software for internal dose assessment in nuclear medicine. J Nucl Med 46:1023–1027
30. Valentin J (2002) Basic anatomical and physiological data for use in radiological protection: reference values. A report of age- and

gender-related differences in the anatomical and physiological characteristics of reference individuals. ICRP Publication 89. Ann ICRP 32:5–265
31. Thomas SR, Stabin MG, Chen CT, Samaratunga RC (1992) MIRD Pamphlet No. 14: a dynamic urinary bladder model for radiation dose calculations. J Nucl Med 33:783–802
32. Mhawech-Fauceglia P, Zhang S, Terracciano L et al (2007) Prostate-specific membrane antigen (PSMA) protein expression in normal and neoplastic tissues and its sensitivity and specificity in prostate adenocarcinoma: an immunohistochemical study using multiple tumour tissue microarray technique. Histopathology 50:472–483
33. Afshar-Oromieh A, Zechmann CM, Malcher A et al (2014) Comparison of PET imaging with a (68)Ga-labelled PSMA ligand and (18)F-choline-based PET/CT for the diagnosis of recurrent prostate cancer. Eur J Nucl Med Mol Imaging 41:11–20
34. Demirci E, Ocak M, Kabasakal L et al (2014) (68)Ga-PSMA PET/CT imaging of metastatic clear cell renal cell carcinoma. Eur J Nucl Med Mol Imaging 41:1461–1462
35. Afshar-Oromieh A, Malcher A, Eder M et al (2013) PET imaging with a [68Ga]gallium-labelled PSMA ligand for the diagnosis of prostate cancer: biodistribution in humans and first evaluation of tumour lesions. Eur J Nucl Med Mol Imaging 40:486–495
36. Eder M, Eisenhut M, Babich J, Haberkorn U (2013) PSMA as a target for radiolabelled small molecules. Eur J Nucl Med Mol Imaging 40:819–823
37. U.S. Department of Health and Human Services Food and Drug Administration Center for Drug Evaluation and Research Center for Biologics Evaluation and Res. The radioactive drug research committee: human research without an investigational new drug application. 2010
38. Deloar HM, Fujiwara T, Shidahara M et al (1999) Internal absorbed dose estimation by a TLD method for 18F-FDG and comparison with the dose estimates from whole body PET. Phys Med Biol 44:595–606
39. Hartmann H, Freudenberg R, Oehme L et al (2014) Dosimetric measurements of (68)Ga-high affinity DOTATATE: twins in spirit - part III. Nuklearmedizin. J Nucl Med 53:211–216
40. Zechmann CM, Afshar-Oromieh A, Armor T et al (2014) Radiation dosimetry and first therapy results with a (124)I/ (131)I-labeled small molecule (MIP-1095) targeting PSMA for prostate cancer therapy. Eur J Nucl Med Mol Imaging 41:1280–1292
41. Afshar-Oromieh A, Avtzi E, Giesel FL et al (2015) The diagnostic value of PET/CT imaging with the (68)Ga-labelled PSMA ligand HBED-CC in the diagnosis of recurrent prostate cancer. Eur J Nucl Med Mol Imaging 42:197–209
42. Kim JH, Lee JS, Kim JS et al (2010) Physical performance comparison of Ga-68 and F-18 in small animal PET systems [abstract]. J Nucl Med 51(Supplement 2):1423